JOURNAL OF GUIDANCE, CONTROL, AND DYNAMICS
Vol. 25, No. 6, November–December 2002

# Modeling and Computing Worst-Case Uncertainty Combinations for Flight Control Systems Analysis

Thomas Mannchen*
*University of Stuttgart, 70550 Stuttgart, Germany*
and
Declan G. Bates† and Ian Postlethwaite‡
*University of Leicester, Leicester, England LE1 7RH, United Kingdom*

**A new technique is presented for generating linear fractional transformation-based uncertainty models for use in the robustness analysis of flight control systems using the structured singular value $\mu$. The proposed approach can be almost fully automated and does not require closed-form linear expressions for how the aircraft dynamics vary as a function of the uncertain aircraft parameters. Only a nonlinear software model of the closed-loop aircraft, which can be efficiently trimmed and linearized numerically, is required. In the proposed technique, linear dependencies of the aircraft dynamics on the uncertain parameters are modeled by a multidimensional regression plane. Additional nonlinear dependencies are modeled using a band structure defined by nonlinearity compensation parameters. The capability of the proposed approach to identify worst-case uncertain parameter combinations is demonstrated through the robustness analysis of a lateral-axis control law for a generic civil transport aircraft. The approach is compared with classical analysis methods via the robustness analysis of a multivariable glide-slope coupler control law for a Boeing 747 transport aircraft.**

## Nomenclature

| | | |
|---|---|---|
| $A, B, C, D$ | = | state-space matrices |
| $C_{L_\beta}$ | = | rolling moment derivative, due to sideslip angle $\beta$ |
| $C_{N_\beta}$ | = | yawing moment derivative, due to sideslip angle $\beta$ |
| $C_{Y_\beta}$ | = | side force derivative, due to side slip angle $\beta$ |
| $F_u$ | = | upper linear fractional transformation |
| $h_e, x_e$ | = | altitude, aircraft position north |
| $J_x, J_z$ | = | inertia in $x$ and $z$ axis |
| $M$ | = | known part of a closed-loop system |
| $m$ | = | mass |
| $n_y$ | = | acceleration in $y$ direction |
| $p, q$ | = | roll rate, pitch rate |
| $\bar{q}$ | = | dynamic pressure |
| $S, b$ | = | wing area and span |
| $\boldsymbol{u}$ | = | input vector |
| $V$ | = | inertial velocity |
| $V_T$ | = | air speed |
| $\boldsymbol{x}$ | = | state vector |
| $x_{\mathrm{cg}}, z_{\mathrm{cg}}$ | = | $x$ and $z$ positions of the center of gravity |
| $\boldsymbol{y}$ | = | output vector |
| $\alpha, \beta, \gamma$ | = | angle of attack, sideslip angle, and flight-path angle |
| $\Delta$ | = | uncertainty in a closed-loop system |
| $\delta p, \delta r$ | = | aileron and rudder deflection |
| $\delta_m$ | = | uncertain parameter, corresponding to mass |
| $\delta_\mu$ | = | structured singular value sensitivity |
| $\mu$ | = | structured singular value |
| $\rho$ | = | stability margin |
| $\bar{\sigma}$ | = | largest singular value |
| $\phi, \theta$ | = | roll angle, pitch angle |

Received 15 November 2001; revision received 1 June 2002; accepted for publication 20 June 2002. 

*Research Engineer, Institute of Flight Mechanics and Control, Pfaffenwaldring 7a.
†Lecturer, Control and Instrumentation Research Group, Department of Engineering, University Road.
‡Professor, Control and Instrumentation Research Group, Department of Engineering, University Road.

## I. Introduction

THE analysis of stability and performance robustness to variations in uncertain aircraft parameters represents a major issue in the flight control law analysis/certification process. The complexity of current aircraft simulation models and control laws, together with the large number of different combinations of flight parameters (e.g., variations in mass, center of gravity positions, inertia, nonlinear aerodynamics, aerodynamic tolerances, air data system tolerances, structural modes, and failure cases) that must be examined throughout the entire flight envelope, makes this analysis a costly and labor-intensive task. As well as identifying the regions of the flight envelope where the aircraft is "safe to fly," a key issue in the control law analysis is to identify worst-case (in terms of the resulting closed-loop stability or performance) combinations of the uncertain parameters. Current approaches that check stability and performance at each point in a gridding of the space of all possible uncertain parameter variations quickly become computationally inefficient as the number of uncertain parameters increases. Moreover, gridding approaches provide no guarantee that the true worst case has in fact been found: In particular, situations where the worst-case parameter combination occurs in the interior of the parameter space could easily be missed.

The technique of $\mu$ analysis[1] has been proposed as a tool that may be used to improve both the efficiency and accuracy of the flight control law analysis task.[2,3] Unlike the gridding approach, $\mu$ provides guarantees that a particular stability or performance property is satisfied over a continuous range of values for each uncertain parameter. Moreover, worst-case values of these parameters may be computed on a frequency-by-frequency basis.

To apply $\mu$-analysis techniques to the flight control law certification problem, a so-called linear fractional transformation- (LFT-) based model of the uncertain closed-loop system must first be generated.[4] Consider a linear time-invariant, closed-loop system that is subject to some unstructured and/or structured type of norm-bounded uncertainty, arranged in the form shown in Fig. 1. It is generally possible to rearrange any such system into the form shown in Fig. 2, where $M$ represents the known part of the system (plant and controller) and $\Delta$ represents the uncertainty present in the system. In effect, extra inputs and outputs are introduced so that the system uncertainty can be considered as part of an external feedback loop.

If $M$ is partitioned compatibly with the matrix $\Delta$, the transfer function of the closed-loop system shown in Fig. 2 is then given by the upper LFT:

$$y = F_u(M, \Delta)r = \left[M_{22} + M_{21}\Delta(I - M_{11}\Delta)^{-1}M_{12}\right]r \quad (1)$$

When it is assumed that the nominal system ($\Delta = 0$) is asymptotically stable and that $\Delta$ is a complex unstructured uncertainty block, the small gain theorem[5] can be used to derive the following result: The closed-loop system is stable if and only if

$$\bar{\sigma}[\Delta(j\omega)] < 1/\bar{\sigma}[M_{11}(j\omega)] \qquad \forall\omega \quad (2)$$

This result defines a stability test for a closed-loop system subject to unstructured uncertainty in terms of the maximum singular value of the matrix $M_{11}$.

Now consider the case where the uncertainty matrix $\Delta$ has a diagonal or block diagonal structure, that is,

$$\Delta(j\omega) = \text{diag}[\Delta_1(j\omega), \ldots, \Delta_n(j\omega)]$$
$$\bar{\sigma}[\Delta_{i=1\ldots n}(j\omega)] \le k_m(j\omega) \quad (3)$$

Again, assume that the nominal system ($\Delta = 0$) is asymptotically stable, and consider the following question: What is the maximum value of $k_m(j\omega)\ \forall\omega$ for which the closed-loop system will remain stable? Applying the small gain theorem to this problem is again possible; however, the result will be conservative because the diagonal structure of the $\Delta$ matrix will not be taken into account. To get a nonconservative solution, the structured singular value $\mu$ was introduced[1]:

$$\mu_{\Delta(j\omega)}[M_{11}(j\omega)]$$
$$:= 1/(\min\{k_m(j\omega) \text{ such that } \det[I - M_{11}(j\omega)\Delta(j\omega)] = 0\}) \quad (4)$$

where $\mu$ defines a stability test of a closed-loop system subject to structured uncertainty in terms of the maximum structured singular value of the matrix $M_{11}$. The problem of calculating the exact value of $\mu$ has been shown to be nonpolynomial time (NP) hard,[6] and so in practice upper and lower bounds are generally computed using various approaches.[2]

In recent years much attention has been paid to the issue of how to generate efficiently accurate (and ideally minimal) LFT-based uncertainty models for complex uncertain systems. See Ref. 2 for an overview. A common assumption among almost all of the approaches suggested is that closed-form analytical expressions relating the aircraft dynamics to the uncertain parameters of interest are available, from which LFT-based uncertainty models may be derived. Such expressions usually take the form of nonlinear equations of motion involving the uncertain parameters, which, when linearized symbolically using dedicated software tools,[7–9] result in linear state-space models whose coefficients depend explicitly on the uncertain parameters. Given state-space models in this form, the generation of accurate, if not always minimal, LFT-based uncertainty models is then relatively straightforward. See Refs. 10–12 for some flight control examples. The main drawbacks of the described approach can be identified as the substantial modeling effort required to relate accurately all of the uncertain parameters to the nonlinear aircraft dynamics and that the symbolically linearized state-space models are generally valid only at and around the relevant operating point in the flight envelope.

In this paper, we present an alternative approach for generating LFT-based uncertainty models that does not require the availability of analytical expressions relating the aircraft dynamics to the uncertain parameters. Only a nonlinear software model of the closed-loop aircraft, which can be efficiently trimmed and linearized numerically for different values of the uncertain parameters, is required. Preliminary results of this research have been published in Ref. 13. The proposed approach allows a significant reduction in the modeling effort required and in general can be applied to complex systems that cannot be satisfactorily described using simple differential-equation-based symbolic models.

The main point of this paper is to show that the proposed approach is a valid alternative procedure, which may be applied when it is not possible to use an exact symbolic approach to LFT modeling. There are two main reasons why it might not be possible to apply the exact approach to a realistic aircraft model:

1) Many nonlinear aircraft models are hybrid in structure, that is, they may be implemented in a block diagram modeling environment such as SIMULINK®, but within various SIMULINK blocks there may be .mex files running FORTRAN or C code. If these files are accessing uncertain aircraft parameters, then it is not possible to use the exact approach at all.

2) Even if the entire model is in pure SIMULINK form, LFT modeling using the exact approach assumes that the linearization of the model can be considered to be independent of the uncertain parameters. If, for example, the angle of attack $\alpha$ is to be considered as an uncertain parameter for the purposes of LFT generation, it will not be valid to use an LFT that is exact only at the nominal value of $\alpha$.

The paper is organized as follows: Section II provides a detailed description of the proposed technique for generating LFT-based uncertainty models. The capability of the proposed method to calculate the worst-case uncertain parameter combination is demonstrated in Sec. III, by comparing $\mu$-analysis results with those produced for an exact symbolic LFT-based uncertainty model of a generic civil transport aircraft model. In Sec. IV, the proposed technique is compared with the classical gridding approach, via the analysis of a glide-slope coupler control law for a more realistic, full nonlinear model of a Boeing 747 aircraft. Finally, some conclusions are presented in the Sec. V.

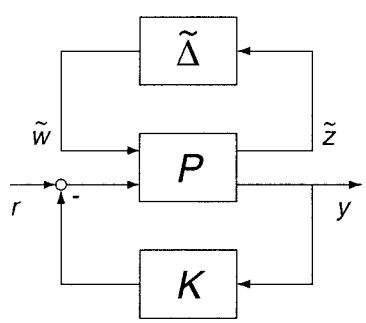


**Fig. 1 Closed-loop system with uncertain plant.**

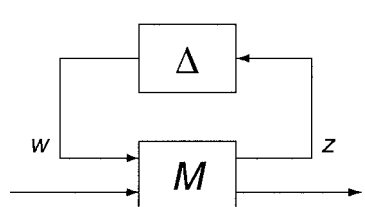


**Fig. 2 Upper LFT uncertainty description.**

## II. LFT-Based Uncertainty Modeling Using Trends and Bands

As shown in Ref. 14, LFT-based parametric uncertainty models may be conveniently derived from a linear state-space representation of the uncertain system of the form

$$\dot{\boldsymbol{x}} = (A_0 + A_1\delta_1 + \cdots + A_n\delta_n)\boldsymbol{x} + (B_0 + B_1\delta_1 + \cdots + B_n\delta_n)\boldsymbol{u}$$
$$\boldsymbol{y} = (C_0 + C_1\delta_1 + \cdots + C_n\delta_n)\boldsymbol{x} + (D_0 + D_1\delta_1 + \cdots + D_n\delta_n)\boldsymbol{u} \quad (5)$$

The matrices $A_0$, $B_0$, $C_0$, and $D_0$ describe the nominal system, whereas $A_k$, $B_k$, $C_k$, and $D_k$, $k = 1, \ldots, n$, describe deviations from the nominal system depending on the normalized physical uncertain parameter $\delta_k$ with $-1 \le \delta_k \le 1$.

In this paper, we focus primarily on the problem of generating state-space representations of the type given in Eq. (5) from the original nonlinear simulation model of the aircraft. Various methods can be used to tackle this problem. The first possibility is to use a Taylor-series approximation around a chosen equilibrium point. For example, the $A$ matrix depending on the $k$th parameter can be written as

$$A = \underbrace{A(\delta_k = 0)}_{A_0} + \underbrace{\left.\frac{\partial A}{\partial \delta_k}\right|_{\delta_k = 0}}_{A_k} \delta_k \tag{6}$$

where the partial derivatives in expression (6) can be computed numerically using finite differences. The advantage of this method is that it uses a standard procedure and that the partial derivatives can be calculated easily. This formulation, however, is valid only for regions in the flight envelope where uncertainty results in small or linear variations in the aircraft model. In the case of highly nonlinear dependence of the state-space representation on the uncertain parameters, linearization intervals become so small that the parameter envelope must be split into many small regions. Moreover, without exact knowledge of the system, the determination of the linearization intervals, the computation of the derivatives, and the choice of appropriate equilibrium points are often difficult.

A second approach to the problem of generating LFT-based uncertainty models in the form given by Eq. (5) is the so-called min–max technique.[9,15] Here, the values of the system-matrix elements are evaluated so that the minimum and the maximum value within the given parameter range are identified elementwise. For example, one element $a_{ij}$ of the $A$ matrix can be written as

$$a_{ij} = a_{ij_0} + a_{ij_{\text{minmax}}} \delta_{a_{ij_{\text{minmax}}}} \tag{7}$$

with

$$a_{ij_0} = \left(a_{ij_{\max}} + a_{ij_{\min}}\right)/2, \qquad a_{ij_{\text{minmax}}} = \left(a_{ij_{\max}} - a_{ij_{\min}}\right)/2$$
$$-1 \le \delta_{a_{ij_{\text{minmax}}}} \le 1 \tag{8}$$

Note that for each varying element of the state space matrices $A$, $B$, $C$, and $D$ an individual $\delta$ is needed. Note further that these $\delta$ are fictitious and have no physical meaning. The method is straightforward to implement, but it can lead to conservatism because possible joint parametric dependencies in the state-space model are ignored. Furthermore, because the fictitious $\delta$ do not directly represent the physical uncertain parameters, it is not possible to identify the worst-case combination of these parameters in the resulting $\mu$ analysis.

In this paper we propose a new method for generating LFT-based uncertainty models that is less conservative than the min–max approach and, moreover, allows the computation of worst-case uncertainty combinations in terms of physical uncertain parameters. As with the min–max approach, however, no closed-form expressions (typically linearized equations of motion) involving the physical parameters are required. The key idea of the proposed method is to model the uncertainties using a curve-fitting technique in a least-squares sense. Consider, for example, the element $a_{ij} = f(\delta_k)$ of the matrix $A$ depending on one parameter $\delta_k$. The formulation

$$a_{ij} = a_{ij_0} + a_{ij_k} \delta_k \tag{9}$$

then represents a linear approximation of the dependency of this element on the uncertain parameter $\delta_k$, assuming the coefficients $a_{ij_0}$ and $a_{ij_k}$ are derived using a least-squares fit based on $m$ data pairs $(a_{ij}^1, \delta_k^1), \ldots, (a_{ij}^m, \delta_k^m)$. Figure 3 illustrates both the actual dependency $a_{ij} = f(\delta_k)$ and the approximation $a_{ij} = a_{ij_0} + a_{ij_k}\delta_k$ and shows the $r$th data pair $(a_{ij}^r, \delta_k^r)$, $r = 1, \ldots, m$. For $k = 1, \ldots, n$

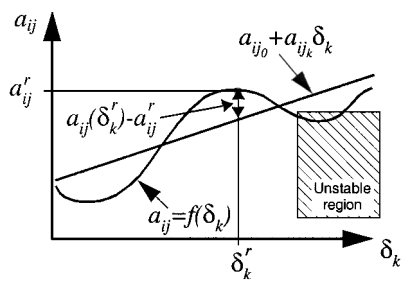


**Fig. 3 Dependence of a matrix element on a parameter; problem of linear approximation.**

uncertain parameters, the equation for the coefficients is then given by

$$\underbrace{\begin{bmatrix} 1 & \delta_1^1 & \ldots & \delta_n^1 \\ 1 & \delta_1^2 & & \delta_n^2 \\ \vdots & \vdots & & \vdots \\ 1 & \delta_1^m & \ldots & \delta_n^m \end{bmatrix}}_{X} \underbrace{\begin{bmatrix} a_{ij_0} \\ a_{ij_1} \\ \vdots \\ a_{ij_n} \end{bmatrix}}_{y} = \underbrace{\begin{bmatrix} a_{ij}^1 \\ a_{ij}^2 \\ \vdots \\ a_{ij}^m \end{bmatrix}}_{z} \tag{10}$$

This usually overdetermined system of equations can be solved for the coefficients in a least-squares sense by solving

$$\boldsymbol{y} = (X^T X)^{-1} X^T \boldsymbol{z} \tag{11}$$

In the case of two uncertain parameters, the curve that was approximated by a line, as in Fig. 3, can then be interpreted as a surface that is approximated by a plane. In the case of $n$ uncertain parameters, the approximation can be interpreted as a multidimensional regression plane.

Note that the implementation of higher-order polynomial fits under this approach is also straightforward. For the work presented in this paper, however, a linear fit was found to be adequate.

Repeating the described procedure for all elements of the state space matrices $A$, $B$, $C$, and $D$ yields a set of parameter-dependent system equations,

$$\dot{\boldsymbol{x}} = (A_0 + A_1\delta_1 + \cdots + A_n\delta_n)\boldsymbol{x} + (B_0 + B_1\delta_1 + \cdots + B_n\delta_n)\boldsymbol{u}$$
$$\boldsymbol{y} = (C_0 + C_1\delta_1 + \cdots + C_n\delta_n)\boldsymbol{x} + (D_0 + D_1\delta_1 + \cdots + D_n\delta_n)\boldsymbol{u} \tag{12}$$

Note that the $\delta$ are now all related to the physical uncertain parameters.

For use in a $\mu$ analysis, these fits must be transformed into an LFT-based uncertainty model. To do so, a state-space representation is created, using the approach proposed in Ref. 14. In a matrix representation, the $M$ block for the linear fit can be assembled in the following manner:

$$\begin{bmatrix} \dot{\boldsymbol{x}} \\ \boldsymbol{z}_1 \\ \vdots \\ \boldsymbol{z}_n \\ \boldsymbol{y} \end{bmatrix} = \begin{bmatrix} A_0 & [A_1 \;\; B_1] & \cdots & [A_n \;\; B_n] & B_0 \\ \begin{bmatrix} I \\ 0 \end{bmatrix} & 0 & \cdots & 0 & \begin{bmatrix} 0 \\ I \end{bmatrix} \\ \vdots & \vdots & & \vdots & \vdots \\ \begin{bmatrix} I \\ 0 \end{bmatrix} & 0 & \cdots & 0 & \begin{bmatrix} 0 \\ I \end{bmatrix} \\ C_0 & [C_1 \;\; D_1] & \cdots & [C_n \;\; D_n] & D_0 \end{bmatrix} \cdot \begin{bmatrix} \boldsymbol{x} \\ \boldsymbol{w}_1 \\ \vdots \\ \boldsymbol{w}_n \\ \boldsymbol{u} \end{bmatrix} \tag{13}$$

When the loop between $[\boldsymbol{w}_1, \ldots, \boldsymbol{w}_n]^T$ and $[\boldsymbol{z}_1, \ldots, \boldsymbol{z}_n]^T$ is closed with the $\Delta$ block, which is of the form

$$\Delta = \operatorname{diag}\left(\delta_1 \begin{bmatrix} I & 0 \\ 0 & I \end{bmatrix}, \ldots, \delta_n \begin{bmatrix} I & 0 \\ 0 & I \end{bmatrix}\right) \tag{14}$$

it can be shown that Eqs. (13) and (14) are an LFT of the system given in Eq. (12) (see Ref. 14).

The method described is a linear approximation of the uncertain system. Therefore, it does not cover nonlinearities in the dependence of state-space matrices on the uncertain parameters. Hence, some unstable combinations could be left out during the $\mu$ analysis, which would make the whole analysis invalid. For instance, assume that a matrix has a varying element $a_{ij}$. As shown in Fig. 3, the unstable region could be left out by the test, if only a linear approximation is used. To include deviations from the linear approximations, additional real nonlinearity compensation parameters (CPs) are added to the existing $\delta$ set (Ref. 9). These take the form of $a_{ij_{\text{CP}}}\delta_{a_{ij_{\text{CP}}}}$, where $a_{ij_{\text{CP}}}$ represents the maximum deviation from the linear representation and $\delta_{a_{ij_{\text{CP}}}}$ is an additional normalized $\delta$. The compensation

parameters add an uncertainty band structure to the trend established by the dependence of the state-space elements on the physical uncertain parameter. Each compensation parameter independently acts on one state-space matrix element. To keep the variation range or the size of the band as small as possible, the least-squares fit is the preferred method for the linear approximation because it minimizes the size of the required band. The equation for one matrix element of the $A$ matrix can now be written as

$$a_{ij} = a_{ij_0} + a_{ij_1}\delta_1 + \cdots + a_{ij_n}\delta_n + a_{ij_{\mathrm{CP}}}\delta_{a_{ij_{\mathrm{CP}}}} \tag{15}$$

The size of the band is chosen to be the maximum error between the linear approximation and the actual value of a matrix element. Figure 3 illustrates this for the $r$th data point. Note that the size of the band depends on the number and locations of the data points $r$. A strategy for choosing an appropriate number of data points is given in Sec. IV. The following equation gives the size of the band for the general case of $n$ parameters:

$$a_{ij_{\mathrm{CP}}} = \max_{r=1,\ldots,m} \left( \left| a_{ij}\left(\delta_1^r, \ldots, \delta_n^r\right) - a_{ij}^r \right| \right) \tag{16}$$

In the proposed technique, therefore, we try to find trends that represent the parameter variations, but allow for nonlinear variations by introducing CPs. In the general case, these trends are modeled by a multidimensional regression plane, which describes the linear variation, and a band structure (CPs), which is limited by planes parallel to the regression plane, above and below, to include nonlinear deviations. The actual value of the uncertain state-space element is then assumed to lie somewhere within this band structure.

Compared with the elementwise min–max approach, which also works with bands, the size of the bands is now reduced, thus decreasing the conservatism of the analysis results (Figs. 4 and 5). Furthermore, the trends introduce $\delta$ with a physical interpretation, which can be used to identify the actual worst-case combination of the physical uncertain parameters.

The nonlinearity CPs $\delta_{\mathrm{CP}}$ are introduced into the LFT by adding four submatrices, $E$, $F$, $G$, and $H$, to the $M$ block representation,

$$\begin{bmatrix} \dot{\boldsymbol{x}} \\ \boldsymbol{z}_1 \\ \vdots \\ \boldsymbol{z}_n \\ \boldsymbol{z}_{\mathrm{CP}} \\ \boldsymbol{y} \end{bmatrix} = \begin{bmatrix} A_0 & [A_1 \;\; B_1] & \cdots & [A_n \;\; B_n] & [E \;\; 0] & B_0 \\ \begin{bmatrix} I \\ 0 \end{bmatrix} & 0 & \cdots & 0 & 0 & \begin{bmatrix} 0 \\ I \end{bmatrix} \\ \vdots & \vdots & & \vdots & \vdots & \vdots \\ \begin{bmatrix} I \\ 0 \end{bmatrix} & 0 & \cdots & 0 & 0 & \begin{bmatrix} 0 \\ I \end{bmatrix} \\ \begin{bmatrix} G \\ 0 \end{bmatrix} & 0 & \cdots & 0 & 0 & \begin{bmatrix} 0 \\ H \end{bmatrix} \\ C_0 & [C_1 \;\; D_1] & \cdots & [C_n \;\; D_n] & [0 \;\; F] & D_0 \end{bmatrix} \cdot \begin{bmatrix} \boldsymbol{x} \\ \boldsymbol{w}_1 \\ \vdots \\ \boldsymbol{w}_n \\ \boldsymbol{w}_{\mathrm{CP}} \\ \boldsymbol{u} \end{bmatrix} \tag{17}$$

with the corresponding $\Delta$ block,

$$\Delta = \mathrm{diag}\left( \delta_1 \begin{bmatrix} I & 0 \\ 0 & I \end{bmatrix}, \ldots, \delta_n \begin{bmatrix} I & 0 \\ 0 & I \end{bmatrix}, \delta_{\mathrm{CP}_1}, \ldots, \delta_{\mathrm{CP}_t} \right) \tag{18}$$

The total number of CPs $t$ is the number of nonlinearly varying elements in the state-space matrices $A$, $B$, $C$, and $D$. The submatrices $E$, $F$, $G$, and $H$ are assembled in the following manner: $E$ and $F$ consist of as many columns as CPs. In each column, the maximum deviation of a matrix element, for example, for matrix $A$: $a_{ij_{\mathrm{CP}}}$, is placed in the position that corresponds to the row index $i$ of the matrix element; all other entries are set to 0. $E$ contains all $a_{ij_{\mathrm{CP}}}$ and $b_{ij_{\mathrm{CP}}}$, whereas $F$ contains all $c_{ij_{\mathrm{CP}}}$ and $d_{ij_{\mathrm{CP}}}$. In a similar manner, $G$ and $H$ are assembled with rows for each compensation parameter, but now the matrix element with the column index $j$ is set to 1; the other elements equal 0.

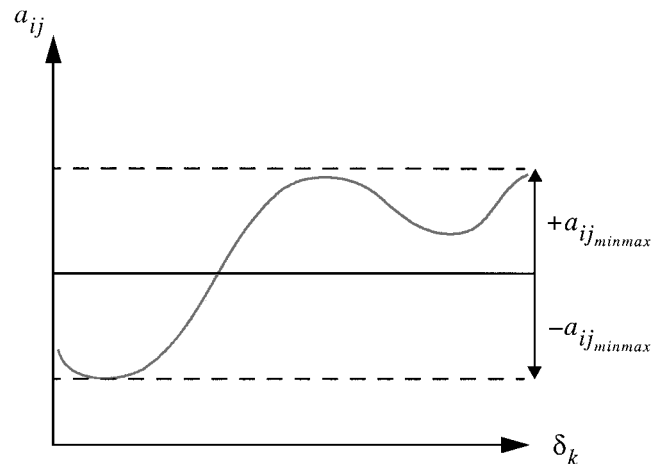


**Fig. 4 Elementwise min–max approach.**

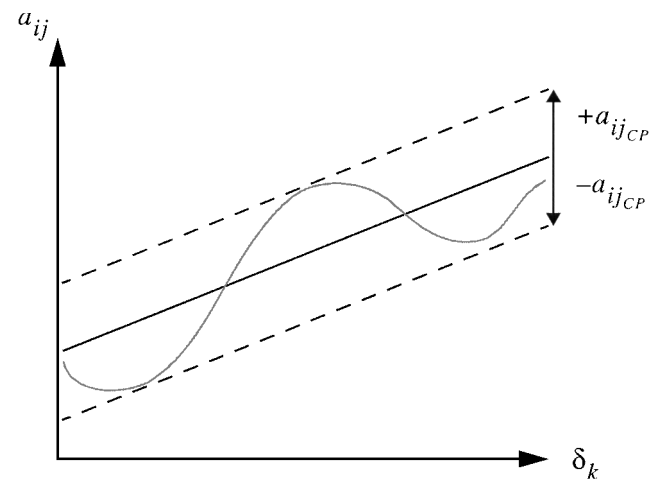


**Fig. 5 Trends and bands approach.**

To illustrate this, an example state-space system with two states, one input, and one output is considered. Assume the matrix elements $a_{11}$ and $d_{11}$ are varying and there is only one physical uncertain parameter. The LFT would then look like

$$\begin{bmatrix} \dot{\boldsymbol{x}} \\ \boldsymbol{z}_1 \\ \boldsymbol{z}_{\mathrm{CP}} \\ \boldsymbol{y} \end{bmatrix} = \begin{bmatrix} A_0 & \begin{bmatrix} a_{11_1} & 0 & 0 \\ 0 & 0 & 0 \end{bmatrix} & \begin{bmatrix} a_{11_{\mathrm{CP}}} & 0 \\ 0 & 0 \end{bmatrix} & B_0 \\ \begin{bmatrix} 1 & 0 \\ 0 & 1 \\ 0 & 0 \end{bmatrix} & 0 & 0 & \begin{bmatrix} 0 \\ 0 \\ 1 \end{bmatrix} \\ \begin{bmatrix} 1 & 0 \\ 0 & 0 \end{bmatrix} & 0 & 0 & \begin{bmatrix} 0 \\ 1 \end{bmatrix} \\ C_0 & \begin{bmatrix} 0 & 0 & d_{11_1} \end{bmatrix} & \begin{bmatrix} 0 & d_{11_{\mathrm{CP}}} \end{bmatrix} & D_0 \end{bmatrix} \cdot \begin{bmatrix} \boldsymbol{x} \\ \boldsymbol{w}_1 \\ \boldsymbol{w}_{\mathrm{CP}} \\ \boldsymbol{u} \end{bmatrix} \tag{19}$$

Note that the all-zeros column (fourth column) and the corresponding fourth row can be deleted but was left in here for clarity. The corresponding $\Delta$ looks like

$$\Delta = \mathrm{diag}\left( \delta_1 \begin{bmatrix} 1 & 0 & 0 \\ 0 & 1 & 0 \\ 0 & 0 & 1 \end{bmatrix}, \delta_{\mathrm{CP}_1}, \delta_{\mathrm{CP}_2} \right) \tag{20}$$

## III. Computation of Worst-Case Parameter Combinations

To demonstrate the capability of the proposed method to find worst-case parameter combinations, a control system[16] for the lateral axis of a civil transport aircraft[2] is considered. The model was chosen because an exact LFT representation,[17] based on a physical model derived from symbolic equations, is available for comparison of worst-case parameter results. The nominal model is characterized by four states $\boldsymbol{x} = [\beta \;\; p \;\; r \;\; \phi]^T$, four outputs $\boldsymbol{y} = [n_y \;\; p \;\; r \;\; \phi]^T$, and two control inputs $\boldsymbol{u} = [\delta p \;\; \delta r]^T$. The linearized lateral equations of motion, at a trim value of the angle of attack and of the pitch angle, $\alpha_0$ and $\theta_0$, are given as

$$\dot{\beta} = \frac{\bar{q}SC_{Y_\beta}}{m}\beta + \left(\frac{\bar{q}SbC_{Y_p}}{2mV_T} + \sin\alpha_0\right)p + \left(\frac{\bar{q}SbC_{Y_r}}{2mV_T} - \cos\alpha_0\right)r + \frac{g}{V}\phi + \frac{\bar{q}SC_{Y_{\delta_p}}}{m}\delta p + \frac{\bar{q}SC_{Y_{\delta_r}}}{m}\delta r \tag{21}$$

$$\dot{p} = \frac{\bar{q}SbC_{L_\beta}}{J_x m}\beta + \frac{\bar{q}Sb^2C_{L_p}}{2J_xV_Tm}p + \frac{\bar{q}Sb^2C_{L_r}}{2J_xV_Tm}r + \frac{\bar{q}SbC_{L_{\delta_p}}}{J_xm}\delta p + \frac{\bar{q}SbC_{L_{\delta_r}}}{J_xm}\delta r \tag{22}$$

$$\dot{r} = \frac{\bar{q}SbC_{N_\beta}}{J_zm}\beta + \frac{\bar{q}Sb^2C_{N_p}}{2J_zV_Tm}p + \frac{\bar{q}Sb^2C_{N_r}}{2J_zV_Tm}r + \frac{\bar{q}SbC_{N_{\delta_r}}}{J_zm}\delta r \tag{23}$$

$$\dot{\phi} = p + \tan\theta_0 r \tag{24}$$

The acceleration at the center of gravity is given by

$$n_y = -\frac{V}{g}\left(\frac{\bar{q}SC_{Y_\beta}}{m}\beta + \frac{\bar{q}SbC_{Y_p}}{2mV_T}p + \frac{\bar{q}SbC_{Y_r}}{2mV_T}r + \frac{\bar{q}SC_{Y_{\delta_p}}}{m}\delta p + \frac{\bar{q}SC_{Y_{\delta_r}}}{m}\delta r\right) \tag{25}$$

A second-order actuator is included at the aileron control input $\delta p$ and a third-order actuator at the rudder input $\delta r$. See Ref. 2 for details of the model and the values of the constants in the preceding equations. As suggested in Ref. 17, uncertainties are introduced in the mass and in the 14 stability derivatives (Table 1). Each uncertain parameter is allowed to vary within $\pm 10\%$ of its nominal value.

A constrained static output feedback law was synthesized using $H_\infty$ loop shaping techniques.[16] The control input is an output feedback of the type

$$u = -\begin{bmatrix} k_1 & 0 & 0 & 0 \\ 0 & k_2 & k_3 & k_4 \end{bmatrix} y \tag{26}$$

**Table 1 Worst-case parameter combinations for T&B and exact LFT, for T&B bands and exact LFT with reduced number of parameters, and $\mu$ sensitivities for T&B and exact LFT**

| Parameter | $\delta_{\mathrm{T\&B}}$ | $\delta_{\mathrm{exact}}$ | $\delta_{\mathrm{T\&B,red}}$ | $\delta_{\mathrm{ex,red}}$ | $\delta_{\mu,\mathrm{T\&B}}$ | $\delta_{\mu,\mathrm{exact}}$ |
|---|---|---|---|---|---|---|
| $m$ | 1.000 | 1.000 | 1.000 | 1.000 | 0.226 | 0.108 |
| $C_{Y_\beta}$ | −1.000 | −1.000 | −1.000 | −1.000 | 0.237 | 0.200 |
| $C_{Y_p}$ | 0.572 | −0.409 | —— | —— | 0.000 | 0.000 |
| $C_{Y_r}$ | −0.742 | −0.892 | —— | —— | 0.000 | 0.000 |
| $C_{Y_{\delta_p}}$ | 0.981 | 1.000 | 1.000 | 1.000 | 0.022 | 0.020 |
| $C_{Y_{\delta_r}}$ | 0.999 | 1.000 | 0.999 | 1.000 | 0.012 | 0.010 |
| $C_{L_\beta}$ | 1.000 | 1.000 | 1.000 | 1.000 | 0.219 | 0.167 |
| $C_{L_p}$ | −0.919 | −0.971 | —— | —— | 0.000 | 0.000 |
| $C_{L_r}$ | −0.941 | −0.889 | —— | —— | 0.001 | 0.001 |
| $C_{L_{\delta_p}}$ | −1.000 | −1.000 | −1.000 | −1.000 | 0.139 | 0.116 |
| $C_{L_{\delta_r}}$ | −1.000 | −1.000 | −1.000 | −1.000 | 0.075 | 0.059 |
| $C_{N_\beta}$ | −0.946 | −0.273 | −0.969 | −0.310 | −0.001 | 0.011 |
| $C_{N_p}$ | 0.681 | 0.111 | —— | —— | 0.000 | 0.000 |
| $C_{N_r}$ | −0.677 | −0.801 | —— | —— | 0.000 | 0.000 |
| $C_{N_{\delta_r}}$ | −1.000 | −0.949 | −0.999 | −0.912 | 0.007 | 0.006 |

The LFT uncertainty model for the closed-loop system is given by the relation

$$\begin{bmatrix} n_y \\ p \\ r \\ \phi \end{bmatrix} = F_u[M(s), \Delta]\begin{bmatrix} \delta p \\ \delta r \end{bmatrix} \tag{27}$$

with the structure of $\Delta$ depending on the LFT-generation method. LFT representations derived using three different methods are compared. The first LFT is referred to as the exact LFT because it is based on a representation of the symbolic equations and the uncertain parameters in SIMULINK block diagram form. The method is described in detail in Ref. 17 and, thus, details will not be given here. We note, however, that the process of generating an LFT-based uncertainty model using this method was quite tedious and time consuming, even for this simple academic aircraft model. To reduce the number of repeated $\delta$, the mass was factored out of the equations of motion. The $\Delta$ associated with the resulting LFT consists of 18 real $\delta$, of which 4, corresponding to the mass, are repeated. The second LFT is obtained using the min–max approach described in the preceding section. The resulting $\Delta$ consists of 19 real $\delta$ without physical meaning. Finally, the proposed trends and bands (T&B) method yields an LFT with a $\Delta$ matrix consisting of 38 real $\delta$. Of these, 19 $\delta$ correspond to the physical parameters, of which the mass is repeated 5 times. The remaining 19 $\delta$ are compensation parameters with no physical interpretation, other than providing a mechanism for capturing the nonlinear dependence of the state-space matrices on the uncertain physical parameters.

In the following $\mu$ calculations the MATLAB® $\mu$-toolbox[4] has been used to calculate the upper bound (UB) on $\mu$. Because the mixed-$\mu$ lower bound (LB) algorithms contained in the toolbox often yield poor results and can even fail to converge when applied to problems containing only real uncertainties, a method for computing lower bounds on real $\mu$ proposed in Ref. 15 was used. The problem of calculating a lower bound on $\mu$ is formulated as an optimization problem,

$$\min_{x \in \Re^n} \bar{\sigma}(\Delta) \qquad \text{with} \quad \Delta = \mathrm{diag}(\boldsymbol{x}) \tag{28}$$

with the nonlinear inequality constraint

$$\det[I - \Delta M_{11}(j\omega)] \leq \varepsilon \tag{29}$$

where $\varepsilon$ is a small number defined by the user.

The resulting upper and lower bounds on $\mu$ for the three LFTs are shown in Figs. 6 and 7. As expected, the peak value of the $\mu$ upper bound for the exact LFT is the smallest. The min–max-based LFT $\mu$-peak value is approximately double the size of the exact value whereas the proposed trends and bands approach yields a value approximately 50% higher than the exact result. In the first two columns of Table 1, the worst-case parameter combinations corresponding to the peak value of the $\mu$ lower bound for the trends and bands and the exact LFT are given, both normalized to lie between −1 and 1. When the worst-case parameter combination predicted by the trends and bands approach is compared with the actual worst-case parameter combination, note that the values agree in most cases. To analyze the cases of disagreement, the $\mu$-sensitivities[18] for both the trends and bands and the exact LFT are calculated. The $\mu$ sensitivities are defined as

$$\delta_{\mu_i} = \lim_{\Delta\alpha \to 0^+} \left.\frac{\mu[M(\alpha)] - \mu[M(\alpha - \Delta\alpha)]}{\Delta\alpha}\right|_{\alpha = 1} \tag{30}$$

where $\alpha$ is a scalar weight applied to the uncertainty $\delta_i$. The $\mu$ sensitivities allow a comparison to be made between the different elements $\delta_i$ of the $\Delta$ matrix, to find out which elements are contributing most or least to the maximum value of $\mu$.

Based on the $\mu$ sensitivities given in the fifth and sixth columns of Table 1, both the trends and bands and the exact LFTs are reduced to contain only significant $\delta$. The $\mu$ calculation is then repeated for the reduced LFTs. Figure 8 shows a comparison of the $\mu$ bounds for the exact LFT with all $\delta$ and with significant $\delta$ only. The curves are

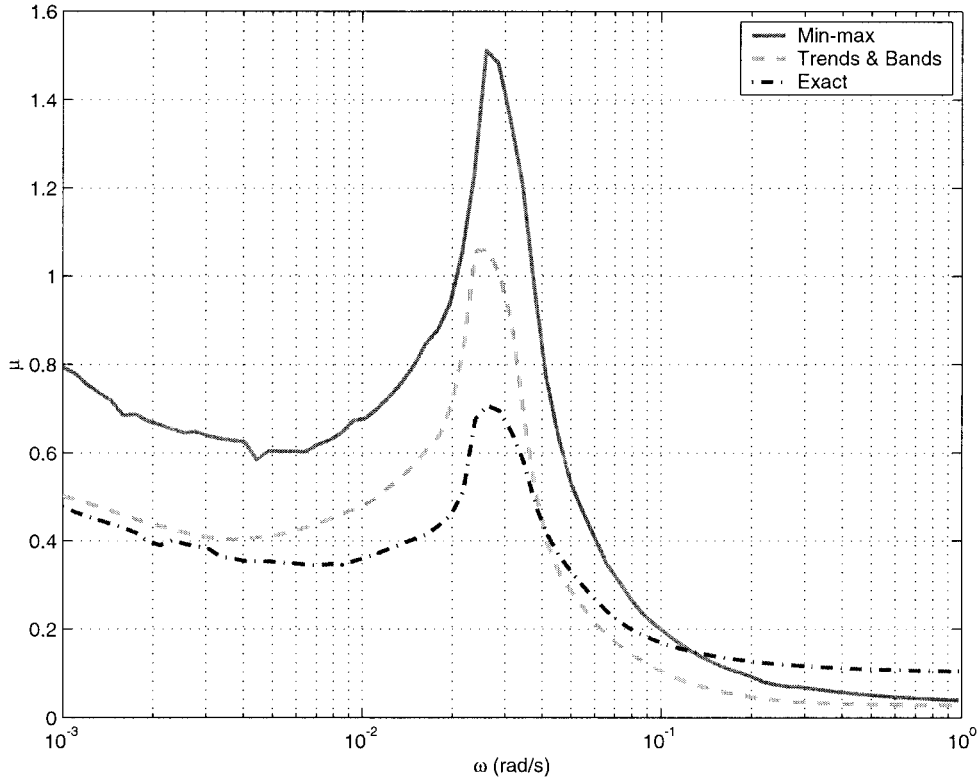


**Fig. 6 Civil transport aircraft example $\mu$ UB using three different LFT creation techniques.**

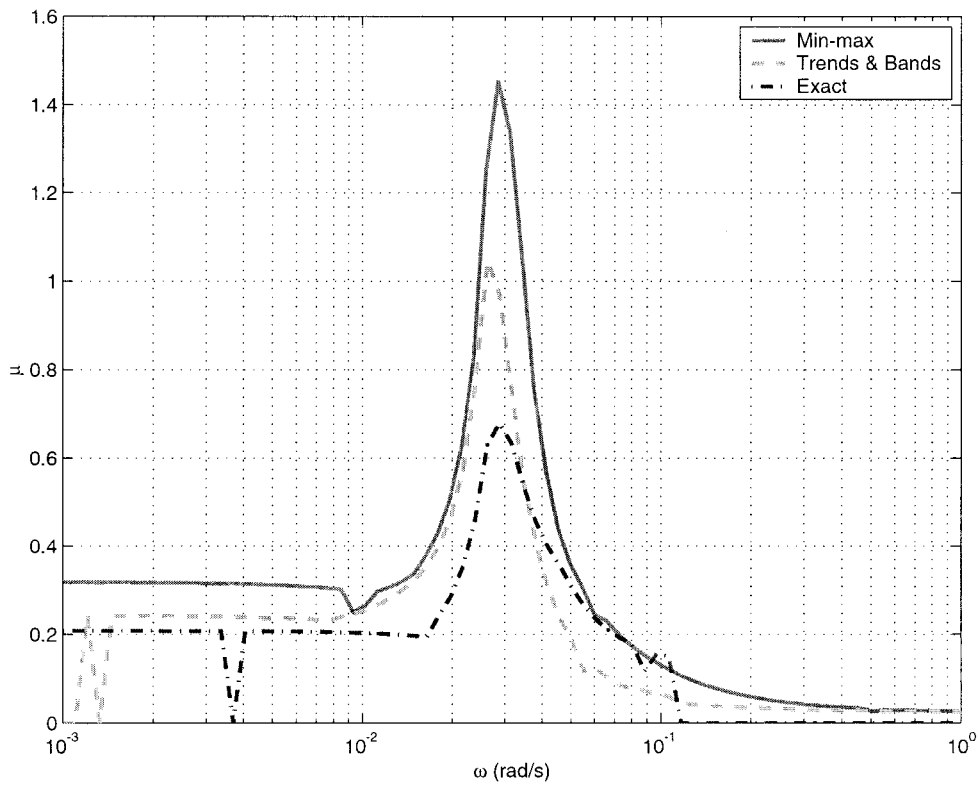


**Fig. 7 Civil transport aircraft example $\mu$ LB using three different LFT creation techniques.**

nearly identical, confirming the result obtained by the $\mu$-sensitivities analysis. The selection of significant $\delta$ and the resulting worst-case parameter combinations are given in the third and fourth columns of Table 1. Now all worst-case parameters suggested by the trends and bands LFT agree with the exact worst-case parameters except for the value of $C_{N_\beta}$. A manual variation of this parameter, however, showed that the dependence of the closed-loop system's eigenvalues on $C_{N_\beta}$ is negligible. This leads to the conclusion that the worst-case value of $C_{N_\beta}$ is mainly influenced by the initial guess in the optimization algorithm and is not really a function of the systems properties, as was already indicated by the very small value of the $\mu$ sensitivity for $C_{N_\beta}$. As a consequence, we conclude that the proposed trends and bands approach allows the correct identification of all relevant worst-case parameters for this example, without the need for the difficult and time-consuming task of generating an exact LFT-based uncertainty model.

Table 2 gives a timing comparison for the exact, the min–max, and the trends and bands approach. The computational effort for calculating the $\mu$ upper bound and the $\mu$ lower bound at the $\mu$ peak frequency is given. Note that only the exact and the trends and bands approach yield a physical worst-case uncertain parameter combination. Clearly, the LFT derived using the exact approach yields the fastest $\mu$ computation time. However, as already noted, there will be many situations when the exact approach cannot be used at all. In such cases, the min–max approach provides an alternative method. At the cost of some increased computation time, the proposed trends and bands approach reduces the conservatism associated with the min–max approach and also allows the computation of the worst-case uncertainty in terms of the physical uncertain parameters.

## IV. Comparison with the Classical Approach

To compare the results based on the proposed method for generating parametric LFT-based uncertainty models with the classical analysis approach, a more realistic model of a large transport aircraft is considered. This model was used to investigate the 1992 Amsterdam aircraft accident[19] and provides an accurate simulation of all flying qualities, characteristics, and hydraulic system operations of a Boeing 747-100/200 aircraft throughout its flight envelope. For example, the nonlinear simulation model includes aerodynamic effects on control surfaces, the lateral control system spoiler program, and a full simulation of the aircraft hydraulic system architecture, as well as the cockpit-to-control-surface and JT9D-7J engine dynamics. Because of the complexity of the model, and because lookup tables are used to evaluate the aerodynamic parameters over the flight envelope, accurate closed-form expressions relating the aircraft dynamics to the uncertain parameters of interest cannot easily be derived. As a consequence, methods to generate LFT-based uncertainty models based on symbolic equations were not considered. Instead, we compare the two alternative options: a classical analysis based on a gridding of the uncertain parameter space and the proposed trends and bands approach to LFT-based uncertainty modeling.

**Table 2 Timing comparison for the generic civil transport aircraft example, $\mu$ UB and $\mu$ LB, for the various approaches to LFT modeling**

| | Timing, s[a] | |
|---|---|---|
| Approach | $\mu$ UB | $\mu$ LB[b] |
| Exact | 28.8 | 23.2 |
| Min–max | 34.2 | 32.6[c] |
| T&B | 110.2 | 188.3 |

[a]Computer time on a standard Pentium II 0.5-GHz processor.
[b]For $\mu$-peak frequency.
[c]LB can be calculated but does not yield a physical worst-case parameter combination with the min–max approach.

In the following analysis, we consider the longitudinal axis only. The control law used for the analysis is a multivariable glide-slope coupler,[20] designed for a flight case of steady horizontal flight at Mach = 0.8 and an altitude of 20,000 ft (6096 m) with each uncertain parameter at its nominal value. The longitudinal-axis equations of motion are characterized by six states $\boldsymbol{x} = [q \;\; V \;\; \alpha \;\; \theta \;\; h_e \;\; x_e]^T$. The inputs are the control column for the elevator and the thrust setting for the four engines. The outputs air speed $V_T$ and flight-path angle $\gamma$ are fed back to the controller. The actuator for the elevator and the engine dynamics are both modeled by second-order systems. Variations in the aircraft mass, as well as center of gravity position in the $x$ and $z$ directions are considered as uncertain parameters. The mass is allowed to vary between 300,000 and 350,000 kg, the range for the $x$ position of the center of gravity is 11–31% of the mean aerodynamic chord, and the $z$ position of the center of gravity is allowed to vary within $\pm 1$ m of its nominal value. These uncertain parameters are represented by the normalized variables $-1 \leq \{\delta_m, \delta_{x\,\mathrm{cg}}, \delta_{z\,\mathrm{cg}}\} \leq 1$, where $+1$ $(-1)$ corresponds to the maximum (minimum) physical value.

To quantify the level of robustness of the considered closed-loop system in the analysis, a measure of robustness has to be defined. To compare meaningfully both analysis approaches, we adopt a classical stability margin, based on a Nichols exclusion region, commonly used in the aerospace industry to evaluate robustness of flight control systems. The closed loop is cut at the sensors at the position indicated in Fig. 9. To avoid the shortcomings of measuring gain

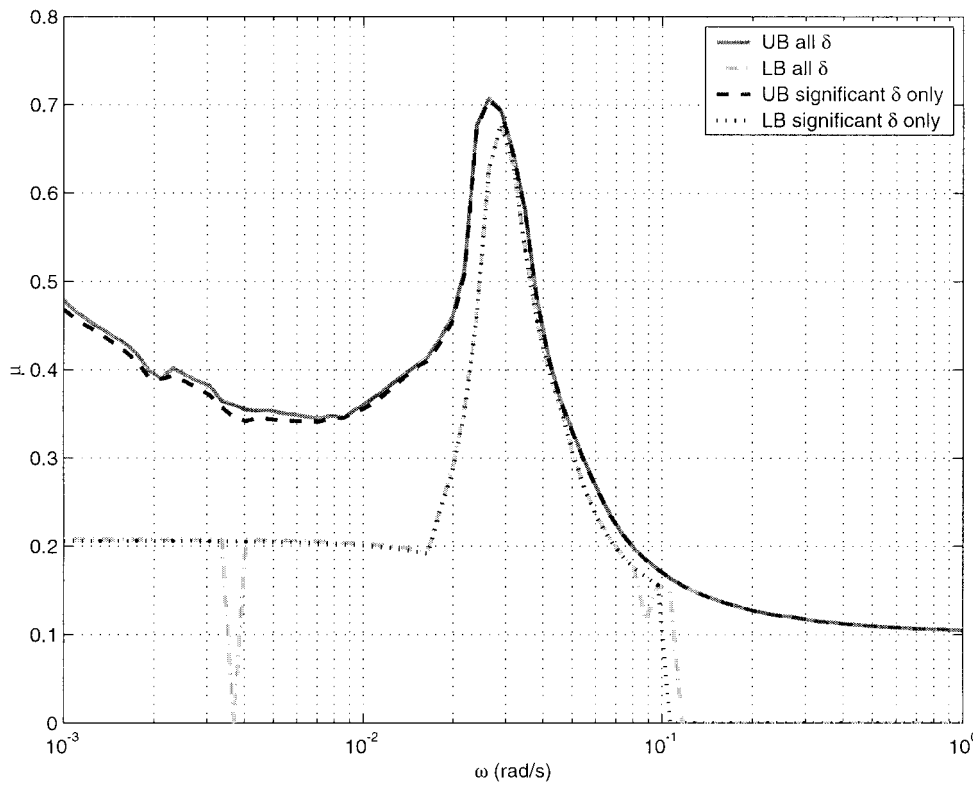


**Fig. 8 Civil transport aircraft example $\mu$ bounds for the exact LFT with all $\delta$ and significant $\delta$ only.**

and phase margins separately, a criterion of simultaneous gain and phase margins is used.[21] As shown in Fig. 10, the stability margin $\rho$ is characterized by an exclusion zone in the Nichols plane for the open-loop frequency response of each loop of the system. A gain offset of 4.5 dB and a phase-offset of 35 deg is defined to correspond to a stability margin of $\rho = 1$. The exclusion zone can be scaled until it touches the Nichols curve resulting in a stability margin of $\rho > 1$ ($\rho < 1$) satisfying (violating) the criterion for each loop of the system. Because all uncertainty parameters are allowed to vary (and affect each loop) simultaneously, this stability margin results in a true multivariable robustness test. Note that the loops can be cut one at a time or simultaneously and that the loop can be broken on the actuator side as well as on the sensor side. Because of space restrictions in this paper, only the results for the $V_T$ feedback loop cut at the sensor output are given.

With the use of the classical approach to study the influence of the uncertain parameters, a grid of 5 points was applied to each parameter, resulting in $5^3 = 125$ uncertain parameter combinations, at which the stability margin $\rho$ has been calculated. The results are given in Fig. 11. In this approach, the worst-case uncertainty parameter combination can be identified to be the maximum possible mass and the center of gravity at its highest and aft limit position. This agrees with our expectations from flight dynamics. The corresponding Nichols curves are given in Fig. 12. In the nominal case the Nichols exclusion criterion is passed, $\rho = 1.24$, whereas the worst-case uncertain parameter combination leads to a violation of the criterion with a stability margin of $\rho = 0.82$. Because of the gridding of the uncertain parameter space, however, no guarantee can be given that the actual worst-case uncertain parameter combination has been found. This becomes particularly important in situations where the worst case is not produced by a combination of the parameters at their vertices.

The effect of the parameters on the time-domain properties of the closed-loop system can be seen in a comparison of the step responses. For example, a step response in $\gamma$ is shown in Fig. 13. Both reference following and decoupling of flight speed and flight-path angle are significantly degraded at the worst-case uncertainty parameter combination.

In the proposed trends and bands approach, LFT-based parametric uncertainty models are generated for the preceding closed-loop system with the three uncertainties, mass and $x$ and $z$ positions of the center of gravity. For the purposes of comparison, both the min–max approach and the trends and bands technique are used to generate uncertainty models. The $\Delta$ associated with the min–max-based LFT uncertainty model consists of 27 fictitious min–max $\delta$. The trends and bands uncertainty model has an associated $\Delta$ composed of 9 repeated $\delta$ for the mass, 9 repeated $\delta$ for $\boldsymbol{x}_{cg}$, 3 repeated $\delta$ for $z_{cg}$, and an additional 27 fictitious $\delta$ associated with the compensation parameters.

The results of a $\mu$-stability test using both LFT-based uncertainty models are given in Fig. 14. Both $\mu$ upper bound peak values, 0.81 for the min–max and 0.78 for the trends and bands approach, guarantee robust stability of the closed-loop system for the considered uncertainty parameter range, as was expected from the analysis using a gridding approach. It can be observed that the conservatism for the phugoid peak is reduced by 30% with the trends and bands approach in comparison with the min–max technique.

To determine the number of data points required for the linear fit in the trends and bands LFT-generation procedure, the following procedure was used: Produce an initial LFT-based uncertainty model using the vertices, that is, the minimum and maximum value of the uncertain parameters only. This gives an uncertainty model characterized by trends only. Plot the resulting $\mu$ upper bound, as given in Fig. 14. Next, increase the number of data points and recalculate and plot the corresponding $\mu$ upper bound. Repeat this until no further increase in the resulting $\mu$ upper bounds toward the min–max-based $\mu$ upper bound result is observed (Fig. 14). The number of points used for the final $\mu$ calculation can then be regarded as being sufficient to cover possible nonlinearities in the dependence of the state-space matrix elements on the uncertainty parameters. Here, five data points for all three uncertainty parameters were used.

To calculate the worst-case uncertainty parameter combination with respect to the Nichols criterion, the exclusion zone is included in the $\mu$ analysis for the trends-and-bands-based LFT uncertainty model as suggested by D. G. Bates, R. Kureemun, and T. Mannchen in "Efficient and Exact Computation of Multivariable

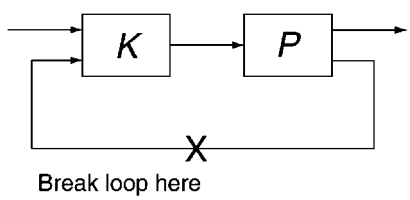


**Fig. 9 Loop broken at the sensors.**

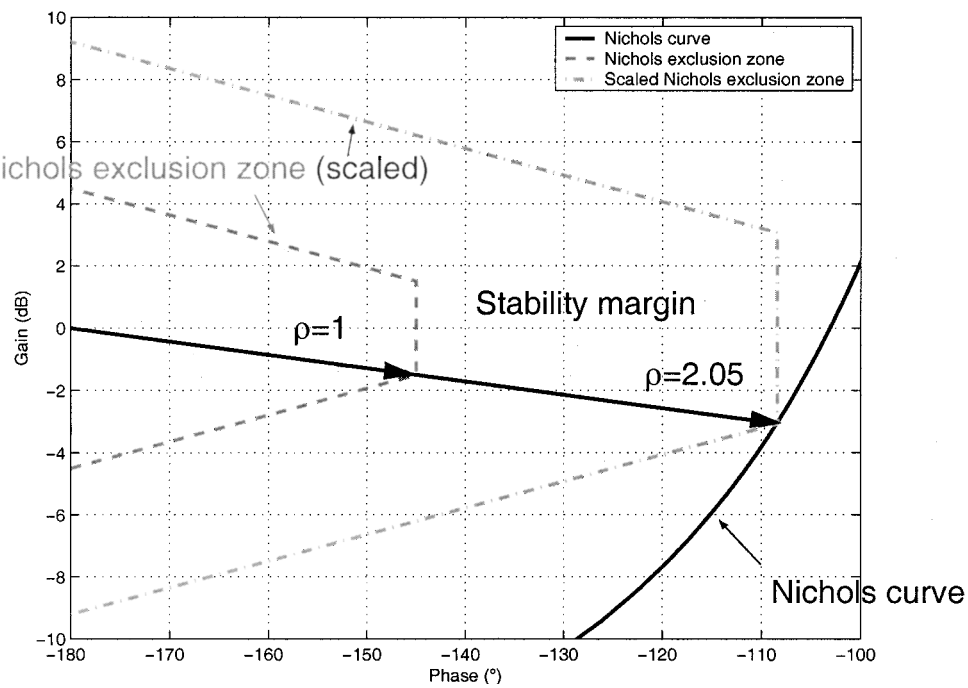


**Fig. 10 Definition of the stability margin $\rho$ as simultaneous gain and phase margin in the Nichols plot.**

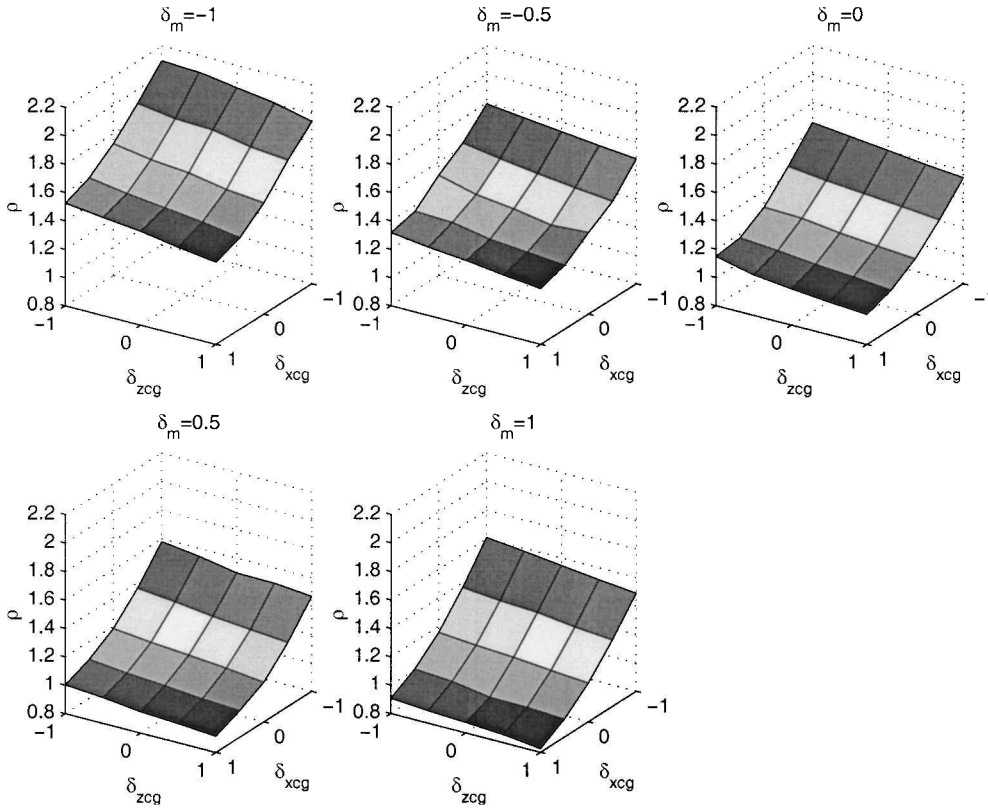


**Fig. 11 Stability margin $\rho$ for the $V$ feedback loop depending on mass and position of center of gravity.**

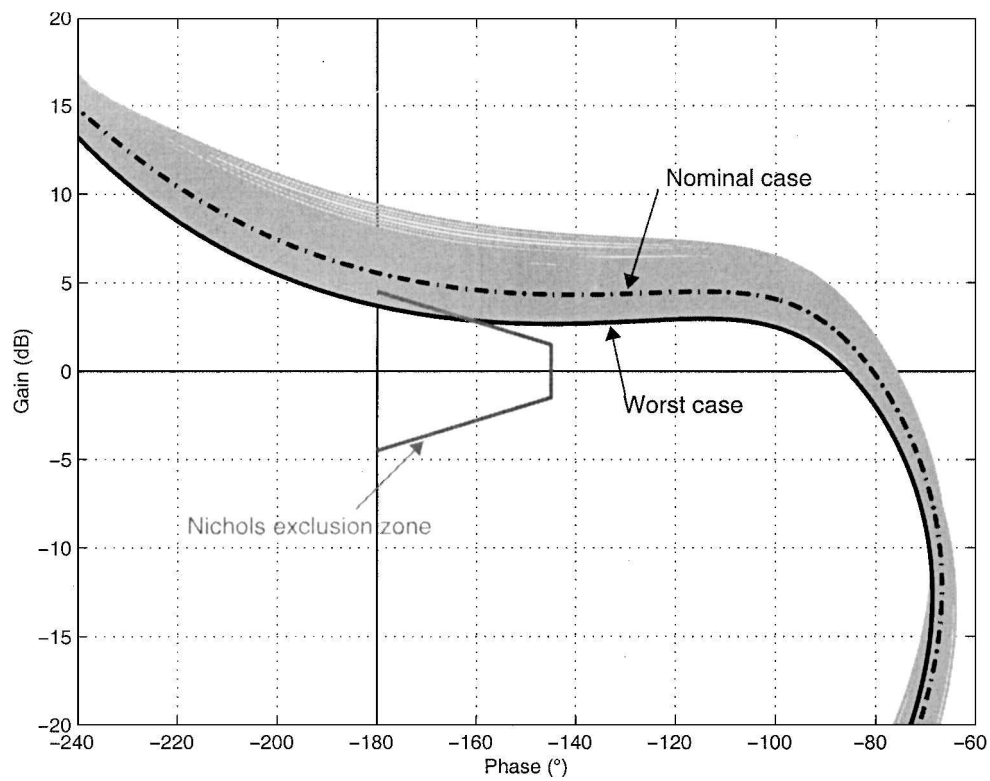


**Fig. 12 Nichols curves for the $V$ feedback loop for a variation of parameters, including nominal and worst case.**

Stability Margins for Aerospace Control Systems" (in preparation). The size of the exclusion zone is then iteratively scaled until a $\mu$-peak value of unity is obtained. The final scaling factor for the Nichols exclusion zone corresponding to a $\mu$-peak value of unity is then equivalent to the minimum (worst-case) stability margin $\rho$ that can be guaranteed for the considered uncertain parameter range. When this approach was used, the value of the stability margin calculated using the trends-and-bands-based LFT uncertainty model was 0.31. Compared to the stability margin of 0.82, calculated with the parameter grid, this result is conservative. However, the associated worst-case uncertainty parameter combination calculated from the $\mu$ lower bound is $\delta_m = 1$, $\delta_{x\,\mathrm{cg}} = 1$, and $\delta_{z\,\mathrm{cg}} = 1$, which is exactly the same as the worst-case uncertainty parameter combination identified with the parameter gridding approach. Thus, although the guaranteed stability margin is conservative, the worst-case uncertainty parameter combination was

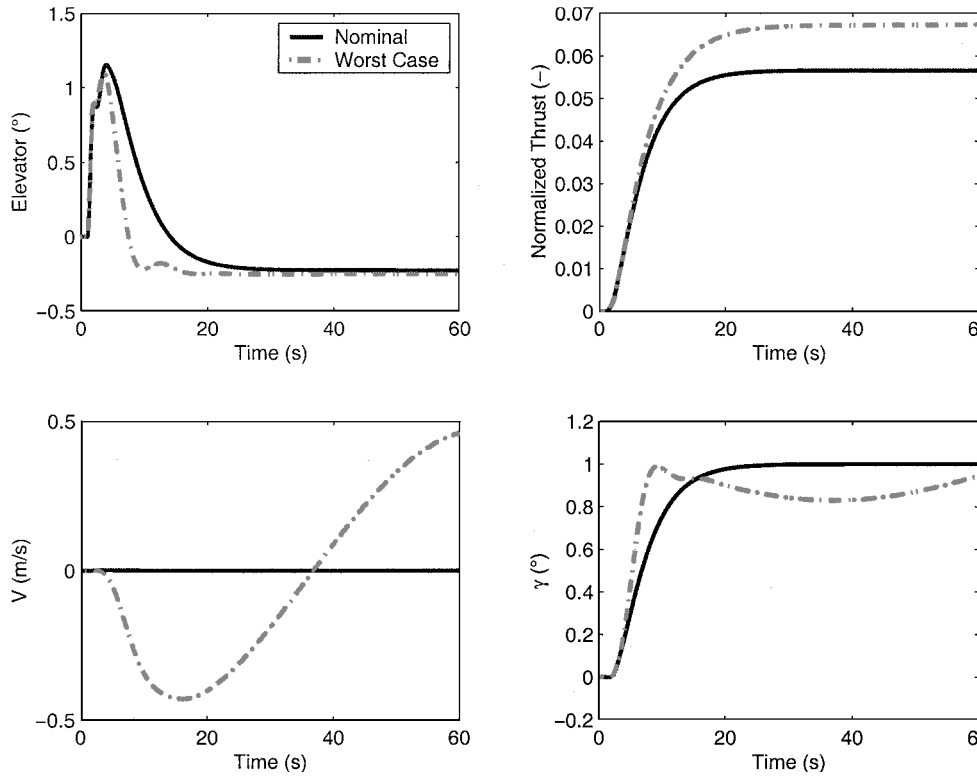


**Fig. 13 Step response on $\gamma$ for the nominal plant (controller design point) and plant at worst-case parameter combination.**

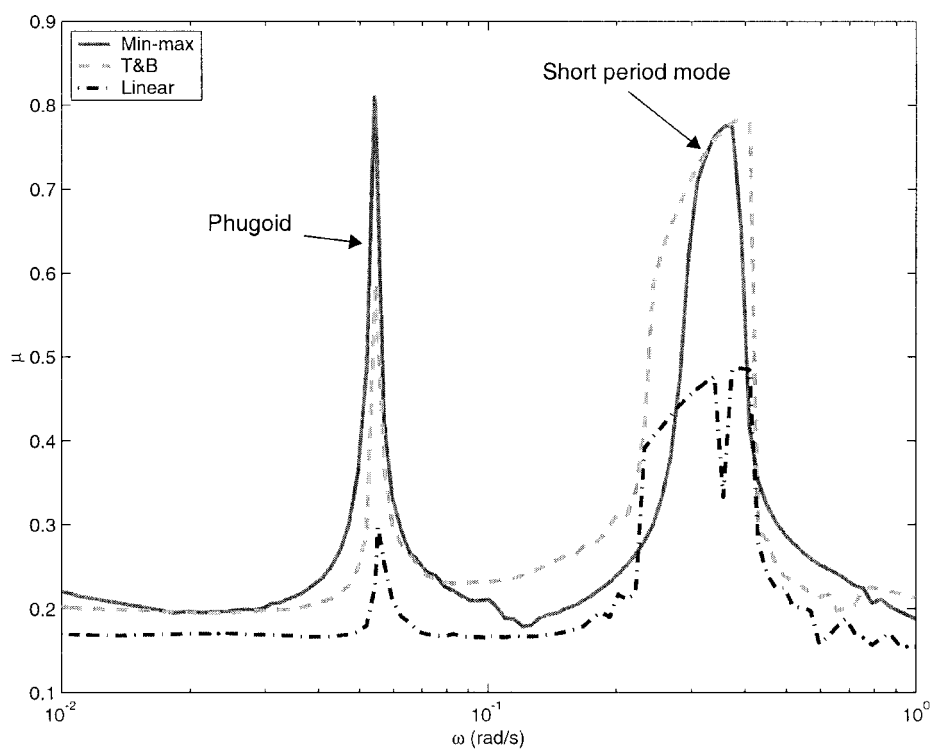


**Fig. 14 Parametric uncertainty models based on min–max, T&B, and linear (trends only) approaches: $\mu$ stability test (UB).**

again found exactly in this example. Furthermore, the LFT-based uncertainty model covers all possible uncertainty parameter combinations, in contrast to the classical approach, which merely evaluates the criterion on a finite number of data points. Thus, situations where the worst-case parameter combination occurred in the interior of the parameter space, which could easily be missed by the classical approach, would be found by the LFT-based uncertainty model.

## V. Conclusions

This paper has introduced a new technique for the generation of LFT-based uncertainty models that are required as inputs for the analysis of flight control systems using the structured singular value $\mu$. In contrast to standard approaches, which use symbolic linearized equations of motion, the proposed approach requires only a nonlinear software model of the aircraft, which can be efficiently trimmed and linearized. In the proposed technique, linear

dependencies (trends) of the aircraft dynamics on the uncertain parameters are modeled by a multidimensional regression plane. Additional nonlinear dependencies are modeled using a band structure defined by nonlinearity compensation parameters. The major advantage of the proposed approach is the capability to identify the true worst-case combination of uncertain parameters with significantly reduced modeling effort. This capability was demonstrated via the analysis of a lateral-axis controller for a simple civil transport aircraft model. The approach was also compared with classical gridding-based analysis methods via the robustness analysis of a multivariable glide-slope coupler control law for a detailed model of a Boeing 747 transport aircraft. For this example, consistent results were obtained in terms of identification of the worst-case parameter combination, although in general only the trends and bands method guarantees robustness for all possible combinations of the uncertain parameters. The major limitation of the proposed approach is that it is prone to be at least somewhat conservative, especially for systems with a strong nonlinear dependence of the state-space representation on the uncertain parameters. On the other hand, the technique allows the process of generating LFT-based uncertainty models to be almost fully automated. More generally, the proposed approach opens up the possibility of applying the powerful $\mu$-analysis theory to large-scale complex systems that cannot be satisfactorily described using simple differential-equation-based symbolic models.

## Acknowledgments

This work was completed while the first author was a Visiting Researcher at the University of Leicester, supported by Engineering and Physical Sciences Research Council. Grant GR/R18871/01. The authors are pleased to acknowledge the contributions to the design of the controllers used in this analysis from Ridwan Kureemun of Leicester University and Melker Härefors of Volvo Aero Corp. Thanks are also extended to Hafid Smaili at the National Aerospace Laboratory (The Netherlands) and the Delft University of Technology Aerospace Engineering Department for the Boeing 747 aircraft model.

## References

[1]Doyle, J. C., "Analysis of Feedback Systems with Structured Uncertainties," *IEE Proceedings*, Vol. 129, Pt. D, No. 6, 1982, pp. 242–250.

[2]Ferreres, G., "A Practical Approach to Robustness Analysis with Aeronautical Applications," *Kluwer Academic*, New York, 1999, Chap. 2.

[3]Doll, C., Ferreres, G., and Magni, J.-F., "$\mu$ Tools for Flight Control Robustness Assessment," *Aerospace Science and Technology*, Vol. 1, No. 3, 1999, pp. 177–189.

[4]Balas, G. J., Doyle, J. C., Glover, K., Packard, A., and Smith, R., "$\mu$-Analysis and Synthesis Tool-box," *MathWorks*, Natick, MA, 1995, Chap. 4.

[5]Skogestad, S., and Postlethwaite, I., *Multivariable Feedback Control*, Wiley, Chichester, England, U.K., 1996, Chap. 8.

[6]Braatz, R., Young, P., Doyle, J. C., and Morari, M., "Computational Complexity of $\mu$ Calculation," *IEEE Transactions on Automatic Control*, Vol. 39, No. 5, 1994, pp. 1000–1002.

[7]Terlouw, J., and Lambrechts, P. F., "A MATLAB Toolbox for Parametric Uncertainty Modeling," National Aerospace Lab., TR CR-93455-L, Amsterdam, 1993.

[8]Varga, A., and Looye, G., "Symbolic and Numerical Software Tools for LFT-Based Low Order Uncertainty Modeling," *Proceedings of the IEEE International Symposium on Computer Aided Control System Design*, Inst. of Electrical and Electronics Engineers, New York, 1999, pp. 1–6.

[9]Varga, A., Looye, G., Moormann, D., and Grübel, G., "Automated Generation of LFT-Based Parametric Uncertainty Descriptions from Generic Aircraft Models," Group for Aeronautical Research and Technology in Europe, TR FM(AG08)/TP-088-36, 1997.

[10]Belcastro, C. M., "Uncertainty Modelling of Real Parameter Variations for Robust Control Applications," Ph.D. Dissertation, Univ. of Drexel, Philadelphia, 1994.

[11]Lambrechts, P., Terlouw, J., Bennani, S., and Steinbuch, M., "Parametric Uncertainty Modelling Using LFT's," *Proceedings of the American Control Conference*, American Automatic Control Council, Evanston, IL, 1993, pp. 267–272.

[12]Idan, M., and Shaviv, G. E., "Robust Control Design Strategy with Parameter Dominated Uncertainty," *Journal of Guidance, Control, and Dynamics*, Vol. 19, No. 3, 1996, pp. 605–611.

[13]Mannchen, T., Bates, D. G., and Postlethwaite, I., "Worst-Case Uncertain Parameter Combinations for Flight Control Systems Analysis," International Federation of Automatic Control, Paper 1210, New York, 2002.

[14]Morton, B., and McAfoos, R., "A $\mu$-Test for Real Parameter Variations," *Proceedings of the American Control Conference*, American Automatic Control Council, Evanston, IL, 1985, pp. 135–138.

[15]Hayes, M. J., Bates, D. G., and Postlethwaite, I., "New Tools for Computing Tight Bounds on the Real Structured Singular Value," *Journal of Guidance, Control, and Dynamics*, Vol. 24, No. 6, 2001, pp. 1204–1213.

[16]Bates, D. G., and Kureemun, R., "Aircraft Flight Controls Design Using Constrained Output Feedback: A $H_\infty$ Loopshaping Approach," AIAA Paper 2001-4281, 2001.

[17]Kureemun, R., Bates, D. G., and Hayes, M. J., "On the Generation of LFT-Based Uncertainty Models for Flight Control Law Robustness Analysis," AIAA Paper 2001-5767, 2001.

[18]Braatz, R. D., and Morari, M., "$\mu$-Sensitivities as an Aid for Robust Identification," *Proceedings of the American Control Conference*, American Automatic Control Council, Evanston, IL, 1991, pp. 231–236.

[19]Smaili, M., "Flight Data Reconstruction and Simulation of the 1992 Amsterdam Bijlmermeer Airplane Accident," AIAA Paper 2000-4586, 2000.

[20]Härefors, M., and Bates, D. G., "Integrated Propulsion-Based Flight Control System Design for a Civil Transport Aircraft," Inst. of Electrical and Electronics Engineers, Paper CCA02-116, New York, 2002.

[21]Muir, E. A. M., "Robust Flight Control Design Challenge Problem Formulation and Manual: The High Incidence Research Model (HIRM)," Group for Aeronautical Research and Technology in Europe, TR FM(AG08)/TP-088-4, 1997.